Overpressure sensing through acousto-optics: a comparison between a self-mixing interferometer and an all-fiber Michelson interferometer

Sébastien Maqueda, Julien Perchoux, Clément Tronche, Louis Thamié, Alan Dufourmentel, Marc Genetier, Maylis Lavayssiere, Yohan Barbarin

Overpressure sensing through acousto-optics: a comparison between a Self-Mixing Interferometer and an all-fiber Michelson interferometer

Sébastien Maqueda*[a,b], Julien Perchoux[a], Clément Tronche[a], Louis Thamié[b], Alan Dufourmentel[b], Marc Genetier[b], Maylis Lavayssière[b] and Yohan Barbarin[b]
[a] Université de Toulouse, LAAS-CNRS, CNRS, INPT, 31000 Toulouse, France;
[b] CEA-DAM, GRAMAT, F-46500 Gramat, France;

ABSTRACT

Recent studies have shown that a compact self-mixing interferometer can be used for the characterization of shock waves. It measures dynamically (> 10 MHz) the changes in the refractive index induced by the shock wave. Associated to an appropriate acousto-optic model, the pressure profile is computed with a 34 mbar resolution. In the present work, we compare shock wave induced refractive index variations measurements by another method using a Michelson-type fiber-optic interferometer with phase analysis that has been developed for Photonic Doppler Velocimetry applications. The output signals of this system are processed in triature, which consists in analyzing the phase shift between the three interferometric signals. This bulkier system provides, in theory, a better resolution than the self-mixing interferometry sensing scheme. In the present paper, we compare these two optical methods to measure a shock wave pressure through experiments that were carried out with an open shock tube instrumented with commercial, bandwidth limited, pressure sensors. This configuration creates a spherical shock wave similar to those observed during on-field experiments with explosives. We describe the two measurement systems and the experimental setup design used for overpressure characterizations. Both sensing approaches have been carried out in the same experimental conditions and with shock wave pressure peak amplitudes of a few bars. We detail the two types of signal processing and we discuss the results obtained with the two optical methods, which are also compared to a piezoelectric reference sensor.

Keywords: Shock wave, Self-mixing interferometer, Laser sensor, Acousto-optics sensor, Michelson Interferometer, Optical fiber, Overpressure, Shock tube

1. INTRODUCTION

In the field of detonic, shock wave characterization in the atmosphere requires precise dynamic overpressure sensors. The overpressure profile at a given distance from the explosion point is determined by several parameters: the shock wave time of arrival, the overpressure peak amplitude, the duration of the positive phase (the duration between the arrival of the shock front and when overpressure is back to zero), and the positive impulse (the overpressure integral of the positive phase). The sensor should be able to measure within 10 to 100 ns an abrupt increase of pressure up to a peak of several bar or even a few tens of bar, followed by an exponential decrease down to the ambient pressure. The positive pressure decay varies between a few hundreds of microseconds and several milliseconds. This decrease presents then a negative phase much slower (up to a second) before returning to atmospheric pressure. The commercial pressure sensors used for these dynamic measurements usually rely on piezoelectric [1] or piezoresistive [2] technologies. The main constrain of these sensors is their bandwidth which is limited to few MHz for the fastest of them; other intrinsic problems of blast pressure measurements were illustrated by Guerke in 1990 [3].

Optical sensors present potential advantages in dynamic pressure measurements, including superior bandwidth, long-distance signal communication, and immunity to electromagnetic interferences. In this paper, two optical approaches for dynamic measurement are proposed: Self-Mixing Interferometer (SMI) [4] and Michelson fiber-optic interferometer [5]. These methods are well-known for displacement or velocity measurement of a target, both measuring external distance variations between the optical sensor output lens and the target. Here, the purpose is to fix the external distance and record the variations of the optical path induced by the shock wave.

*sebastien.maqueda@cea.fr

For both methods, the laser beam is perpendicular to the shock wave propagation and pointing at a distant reflector; it probes the pressure level in between, relying on changes in refractive index as the measured physical parameter. A robust physical model is necessary to derive overpressure as a function of time.

Throughout this article, we present these two optical methods applied to changes in the refractive index measurement with the physics underlying the working principle of the SMI and the Michelson interferometer with phase analysis. The following section outlines the experimental setup of an open shock tube, offering controlled pressure profiles suitable for prototype sensor characterizations. Shadowgraphy was also performed outside the shock tube in order to observe the shock wave shape and its propagation at the shock tube exit. That technique was an added diagnostic to observe the refractive index behavior along the laser beam and better understand the results obtained by the optical sensors. Therefore, optical results are discussed and compared to reference piezoelectric sensors.

2. PRINCIPLES AND METHODS

2.1 SMI principle with fringe counting signal processing

The phenomenon of wave interference within a laser cavity, triggered by optical feedback from a distant reflector or scatterer, leads to alterations in the laser's emitted power and wavelength. Since Lang and Kobayashi's pioneering work [6], the modeling of self-mixing interferometry has been well-developed, extending laser rate's equations to incorporate the re-entry of backscattered waves into the laser cavity. The intricate coupling between the phase and amplitude of the laser's electric field implies a complex, nonlinear relationship between the external cavity's round-trip time and the laser's emitted power. Observing interferometric signals while monitoring laser power or junction voltage reveals a periodic fringe pattern akin to traditional interferometers, where each fringe signifies a $\lambda/2$ variation in the optical path during the external cavity round-trip. The relationship between laser Power under FeedBack (P_{FB}) and the phase shift of the reinjected light wave $\phi_{FB} = 2\pi\nu_{FB}\tau_{ext}$ is expressed as (1).

$$P_{FB} = P_s(1 + m \cdot \cos\phi_{FB}) \tag{1}$$

where τ_{ext} denotes the external cavity's round-trip time, P_s represents the standalone laser power, and m signifies the modulation index, largely depending on the reinjected power to emitted power ratio [7,8].

We recently demonstrated its capability to measure air overpressure in a shock tube utilizing the acousto-optic effect [9]. Here, the laser irradiates a target at a fixed distance L_{ext} and variations in the refractive index δn, induced by shock waves in the external cavity, affect the phase shift ϕ_{FB}, with τ_{ext} decomposed into a constant term τ_0 and a time-varying term $\delta\tau(t)$ as in (2).

$$\delta\tau(t) = \frac{2 \cdot L_{ext}}{c}\delta n(t) \tag{2}$$

As mentioned in the previous paragraph, the resulting SMI signal shows fringes, which signifies fluctuations in the optical path. The signal processing consists in counting each fringe in order to have the fringe number as a function of time $N_{fringes}(t)$, thus the expression of the refractive index variation $\delta n(t)$ is given by (3):

$$\delta n(t) = \frac{\lambda}{2 \cdot L_{ext}} \cdot N_{fringes}(t) \tag{3}$$

In our field of detonic applications, δn is then converted into an overpressure ΔP with the help of an acouto-optic model described in [9]. The wavelength used is 1550 nm in order to have a Class 1 laser system with laser optical power inferior to 10 mW.

2.2 All-fiber Michelson interferometer principle with triature phase analysis

Since 2000's, compacter fiber-based systems known as Photonic Doppler Velocimetry (PDV) [10, 11] systems are used at telecom wavelength near 1550 nm. High-speed PDV systems (up to 10 km/s) use directly Short-Time Fourier Transform (STFT) for the signal processing of the Doppler fringes. When the time resolution gets too limited by the interference fringe size, slightly modified PDV systems are used with a signal processing based on phase analysis [12-14] (also known as a Push-Pull scheme).

In this paper, the PDV system used has an homodyne triature scheme with three phases analysis, the design of the system can be found in [5] and [14] at 532 nm. An all-fiber Michelson interferometer with triature phase analysis consists in

acquiring three interferometric signals using a 3x3 fiber coupler leading to three phases shifted by 120°. The recorded signals from the photoreceivers are (4):

$$\begin{cases} I_1(t) = I_0(t)\cos\left[4\pi \cdot \frac{\delta n(t)\cdot L_{ext}}{\lambda} + \Delta\varphi\right], \\ I_2(t) = I_0(t)\cos\left[4\pi \cdot \frac{\delta n(t)\cdot L_{ext}}{\lambda} + \Delta\varphi + \frac{2\pi}{3}\right], \\ I_3(t) = I_0(t)\cos\left[4\pi \cdot \frac{\delta n(t)\cdot L_{ext}}{\lambda} + \Delta\varphi - \frac{2\pi}{3}\right], \end{cases} \quad (4)$$

with $I_0(t)$ the amplitude voltage of experimental signals and $\Delta\varphi$ the initial phase shift between the output signals of the reference arm and probe arm of the Michelson interferometer. By combining these signals as in (5):

$$\begin{cases} S_1(t) = -3\frac{I_2(t)+I_3(t)}{I_1(t)+I_2(t)+I_3(t)}, \\ S_2(t) = \sqrt{3}\frac{I_3(t)-I_2(t)}{I_1(t)+I_2(t)+I_3(t)}, \end{cases} \quad (5)$$

the expression of the refractive index variation $\delta n(t)$ is given by the following relationship:

$$\delta n(t) = \frac{\lambda}{2\cdot L_{ext}} \cdot \frac{1}{2\pi} \cdot \arctan\left(\frac{S_2(t)}{S_1(t)+2}\right) \quad (6)$$

Analyzing the phase shift among $I_1(t)$, $I_2(t)$ and $I_3(t)$ gives δn, then converted into an overpressure ΔP with the same acousto-optic model of SMI signals [9].

2.3 Open shock tube for optical interferometers characterization

The setup used for our experiments in order to compare both optical diagnostics was composed of a metrological open shock tube with an inner diameter of 40 mm. The shock tube is composed of two distinct sections: the driver and the driven chambers separated by a diaphragm. The driven section functions as a low-pressure chamber. The experiment's objective is to increase the pressure within the driver section until the diaphragm bursts. This break initiates a planar shock wave that travels along the driven section [15]. In our experimental configuration, the end of the driven section is open in order to create a spherical shock wave at the exit of the tube, as the Figure 1 (a) shows. The shock wave shape is confirmed by shadowgraphy in the following section.

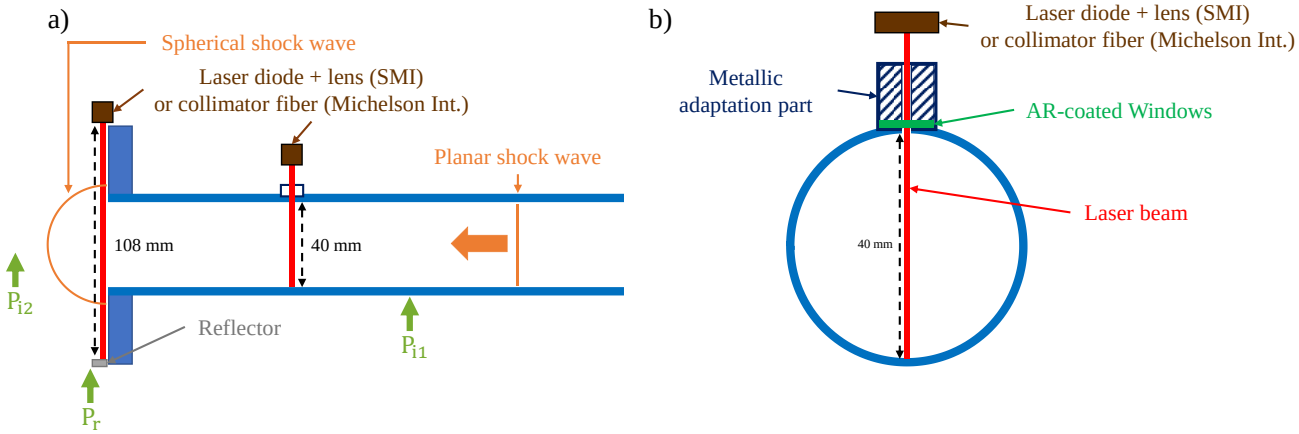

Figure 1: Schematic illustration of the two optical sensors implementation at the end of the shock tube at CEA Facility. Both optical sensors measure pressure in two locations with several external cavity lengths. The reference piezoelectric pressure sensor locations are presented in green arrows (a). Side view of the laser beam within the driven section of the shock tube (b).

The first optical sensor measurement is located trough the driven section, using a drilled-hole dedicated to a piezoelectric pin. A metallic adaptation part was made with an AR coated N-BK7 window in order to allow optical access for the sensors optical beam into the tube. The internal surface of the tube acts here as a reflector. Hence, the segment of the external cavity experiencing a refractive index alteration during the shock wave corresponds to the internal width of the shock tube (40 mm). Theoretically, optical sensors at this location observe a planar shock wave corresponding to the generated pressure step with a constant high level pressure of few bars during several ms (up to 3 ms in the configuration of this

experiment). The second optical sensor was mounted at the end of the tube with a microbeads reflector, thus fixing the external cavity length at 108 mm. This configuration is supposed to be the location of a spherical shock wave. Both interferometers presented in this paper were placed at the two locations during few successive experiments. The SMI is composed of a laser diode (Thorlabs L1550P5DFB) and a collimating lens; the fibered Michelson interferometer is connected to a single mode collimator probe (Oz Optics). Each of these systems operates at 1550 nm. Both optical interferometer's output voltages were recorded at a sampling rate of 20 GSa/s using Keysight DSOS254A high-speed digitizer. The duration of the experiment was 5 ms.

Moreover, commercial reference sensor (PCB Piezotronics 113B26) was placed on the driven section to measure the incident pressure P_{i1} inside the shock tube. Two other pressure sensors (PCB Piezotronics 137A22) were located at the exit of the tube, one at 20 mm of the tube exit in front of the shock wave propagation and the second close to the reflector for reflected pressure measurement (respectively P_{i2} and P_r). Their locations are shown in green on Figure 1.a). These signals were digitized on a GN-412 card mounted on a GEN 7tA HBK data logger with a sampling frequency of 20 MSa/s.

The shock tube's driver section was filled with synthetic air gas, while the driven section was filled with ambient air at atmospheric pressure. A standard cellophane rupture membrane served as the diaphragm separating the two sections. The driver chamber is increased to an average pressure of 7 bar, that creates an incident pressure level between 1.3 and 1.6 bar. Upon rupture, it generates a shock wave with a rise time shorter than 10 ns [16], propagating within the driven section until it exits the tube. This shock wave travels perpendicular to the laser beam axis, changing the air's refractive index in the driven shock tube section, thereby modifying the apparent optical path measured by the laser sensors.

3. RESULTS

Figure 2 shows the results of the SMI sensor for incident pressure measurement in the driven section. The output signal is on Figure 2.a) and the fringes are clearly visible and countable. The fringe counting processing with red circle gives 13 fringes, that are converted into refractive index on Figure 2.b). The SMI sensor observed a refractive index change of $2.5 * 10^{-4}$ when the planar shock wave passes through the laser beam. The SMI sensor resolution corresponds to a single fringe, which is equivalent to a refractive index change of $1.94 * 10^{-5}$. The observed 10-90% rising time is 1.02 µs. This value depends on the shock front wave shape and the laser beam diameter. It will be further discussed when comparing the different types of sensors.

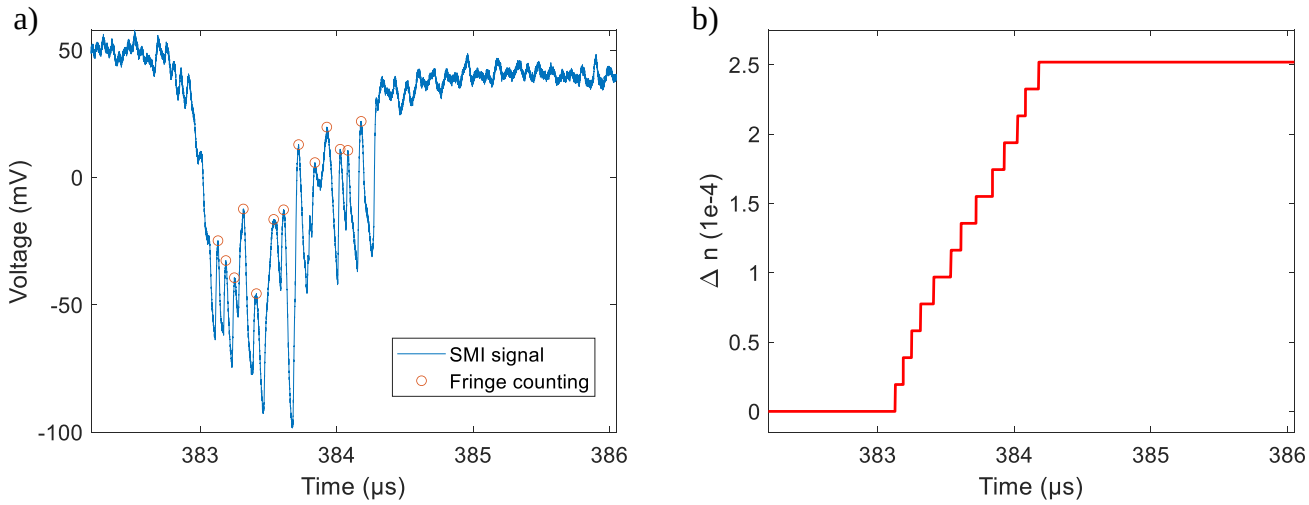

Figure 2 : Zooms on the results for the SMI incident measurement (a) inside the driven chamber of the shock tube in order to observe the refractive index variations induced by planar shock wave (b).

On the Figure 3, results at the shock tube exit made by the SMI sensor are displayed. The fringes on Figure 3.a) do not have the same shape as the previous result for the incident pressure measurement, but most of them have enough amplitude to be counted with our fringe counting algorithm. Here, 17 fringes are obtained when the spherical shock wave interacts with the laser beam, that gives an average index change reaching up to $1.2 * 10^{-4}$ (Figure 3.b). The observed rising time is around 2.19 µs.

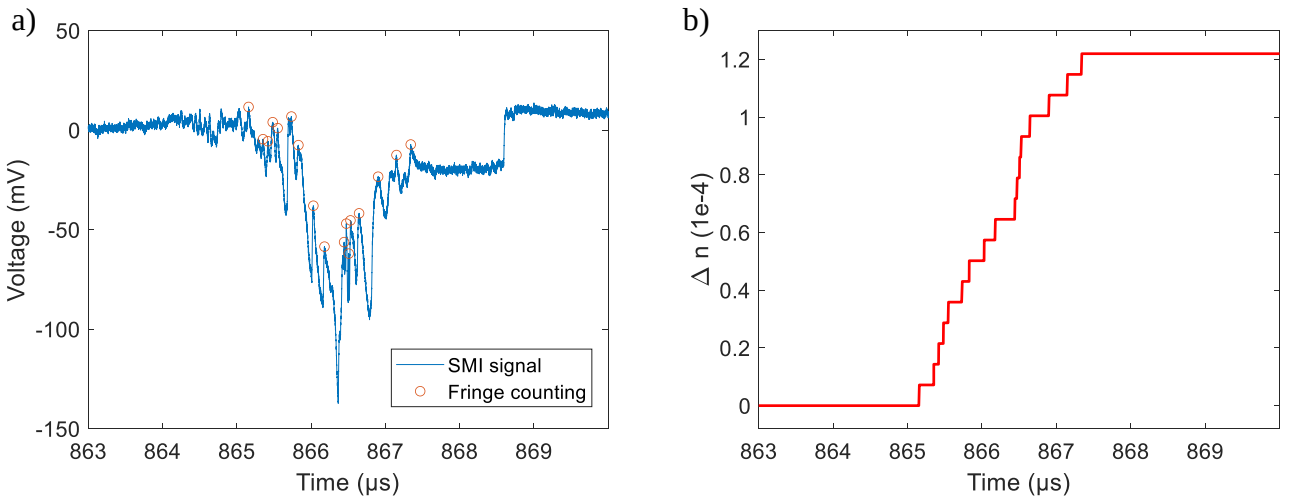

Figure 3 : Zooms on the results for the SMI exit shock tube measurement (a) in order to observe the refractive index variations induced by a spherical shock wave (b).

The Figure 4 shows the results obtained with the Michelson interferometer measuring the index variation induced by the planar shock wave (incident measurement in the driven section). The three outputs are displayed in Figure 4.a). The abrupt increases in amplitudes coincide to the instant where the shock wave passes through the laser beam. The interferences fringes are not clearly visible, but the triature processing provides a refractive index variation plot that reaches a value of $2.5 * 10^{-5}$ (see Figure 4.b)) with a resolution of 10^{-8}. The rising time between 0.0 and $2.3 * 10^{-5}$ is about 750 ns. The shape looks like a step pressure profile, but the refractive index variation is 10 times below the one measured by the SMI sensor for the incident measurement as seen on Figure 2.b) and Figure 4.b).

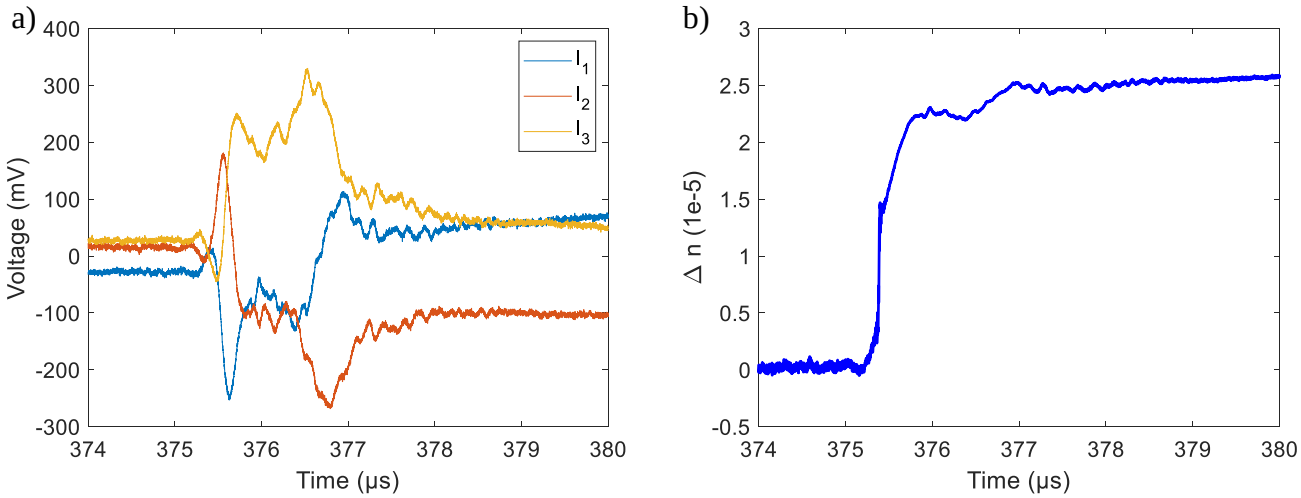

Figure 4 : Zooms on the results for the incident measurement from the Michelson interferometer (a) inside the driven chamber of the shock tube in order to observe the refractive index variations induced by planar shock wave (b).

Figure 5 illustrates a Michelson interferometer data at the exit of the shock tube. Here, the plot on Figure 5.a) shows interferences fringes more pronounced compared to the previous ones for the incident measurement. The triature signal processing shown on Figure 5.b) displays the refractive index reconstitution. It reaches a value around $17 * 10^{-7}$ and the reconstitution appears disturbed. It is difficult to compare the index variation profile as the SMI sensor has a lower resolution. The rising time measured by the Michelson interferometer is about 2.47 µs, which is slightly more than the SMI sensor. At the exit tube, the Michelson interferometer shows a refractive index 70 times lower than the one measured by the SMI sensor. The reason is not clear to us as discussed below.

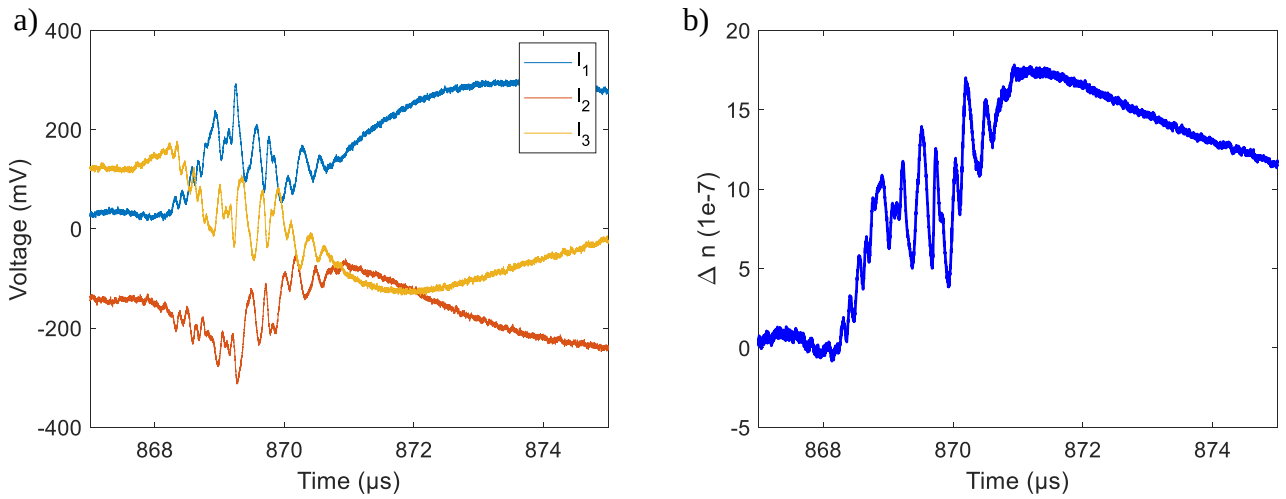

Figure 5 : Zooms on the results for the exit shock tube measurement from the Michelson interferometer (a) in order to observe the refractive index variations induced by a spherical shock wave (b).

In order to compare these results with commercial reference overpressure sensors, we converted all the refractive index with the acousto-optic model described in [9]. Two comparisons with all sensors are plotted on Figure 6.a) and 6.b); green lines are all related to the reference sensors, whose locations are presented on the experimental setup Figure1.a). To better read and compare the amplitudes, data were time offsetted to have all the rising start at the same time. Furthermore, the results displayed were made during different experiments; but the experiments on the shock tube being highly repeatable, these measurements are assumed comparable from one experiment to another.

The Figure 6.a) shows each incident pressure measurement. The reference pressure measurement P_{i1} reaches an overpressure of 1.43 bar, with a rise time of 8.1 µs. The size of the piezoelectric active area and its electric bandwidth explain this longer rise time. The SMI sensor reveals a slightly higher value, with 1.64 bar; and the Michelson interferometer exhibits a low overpressure value of only 131 mbar. Analyzing these results, the SMI sensor pressure value is close to the reference piezoelectric sensor. The slight difference can be explained by an extra fringe during the signal processing and the limited resolution of the SMI sensor in this configuration. The Michelson interferometer completely underestimates the pressure amplitude. It has a correct chronometry and the continuous pressure profile looks like the expected one. One hypothesis is that the Michelson interferometer does not fully integrates the refractive index over the entire length of the beam. Signal processing by STFT did not show any signal at the sound velocity but it has to be further investigated.

Exit tube overpressure measurements shown on Figure 6.b) present the associated pressures to the spherical shock wave. The measurement of P_{i1} was left on that graph in order to display the initial pressure just before the exit of the shock tube. The incident pressure P_{i2}located at 20 mm from the exit reaches an overpressure peak of 1.15 bar with a rising time of 5.4 µs. The peak value is in the correct range but could be slightly underestimated by the piezoelectric sensor. The reflected measurement P_r (54 mm from the center tube exit) presents a slight overshoot due to the resonance frequency excitation of the piezoelectric sensor, but a stable value around 335 mbar can be read. For that reflected pressure sensor, the shock wave velocity vector hits the sensitive element surface perpendicularly and it explains the faster rise time of 950 ns. This orientation regarding the shock wave propagation provides a higher overpressure value measurement that any incident measurement. Both optical sensors measure incident overpressure values along their laser beam. The SMI sensor shows an averaged overpressure value of 710 mbar and the Michelson interferometer of only 86 mbar. The SMI sensor measured a pressure value between P_{i2} and P_r values, this can be explained by the spherical shape of the shock wave front visible by shadowgraphy (Figure 7.b). Indeed, P_{i2} measure the shock wave directly in front of the exit shock tube, thus the shock wave exiting the tube has a maximum of energy at the middle of this front wave. P_r measures the pressure on the side of the sphere, even though this pressure measurement is in a reflection mode, it is lower because the spherical shock wave has less energy at a 90° angle. By analyzing the SMI fringes of Figure 2.a), one can see periodic fringes within a short rise time. In Figure 4.a), the inhomogeneity of the refractive index along the laser beam during the spherical shock leads to a less periodic fringes series which were also more difficult to process. The longer interaction of the spherical shock wave

and the SMI laser beam can explain the rise time of 2.19 µs. In contrast, the Michelson Interferometer gives a pressure value below the expectations. For this spherical shock wave characterization, the interference fringes are more visible on the raw signals (Figure 5.a) and a quick visual counting gives a value of 15, which is not far from the SMI fringe counting Figure3.a). As mentioned for the incident pressure measurement in the shock tube, the results of the Michelson interferometer need to be further investigated.

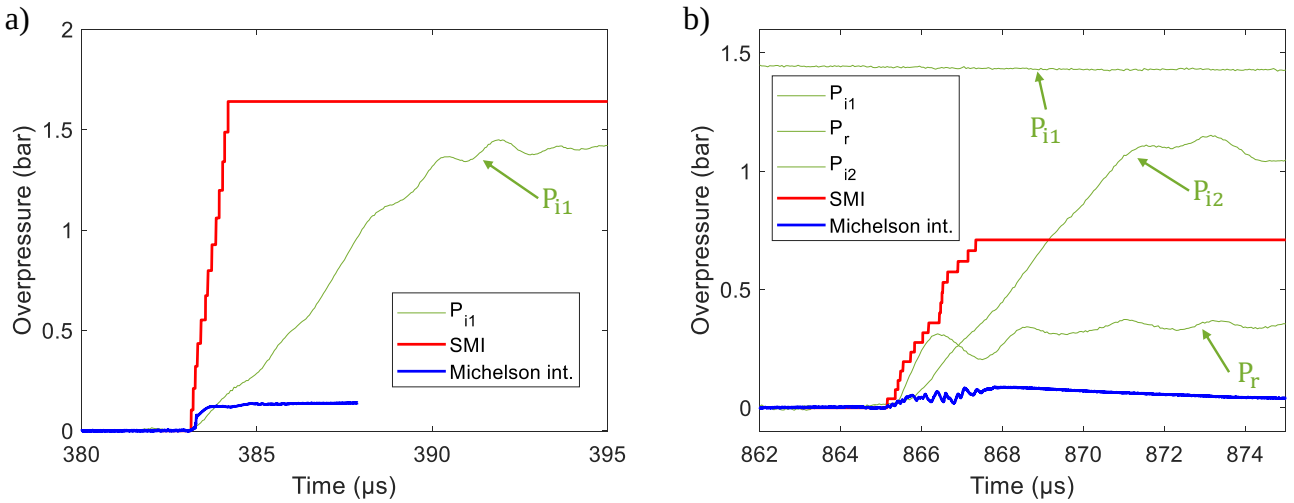

Figure 6 : Comparison between all sensors for the incident measurement (a) and for the exit tube measurement (b)

Shadowgraphy images during an SMI experiment are displayed on Figure 7, showing the spherical shape at the exit of the open shock tube. Shock wave propagation outside the tube begins at around $t_1 = t_0 + 860$ µs, with t_0 the setup trigger time. The time is in correlation with optical measurements made before and reinforces the fact that the fringes (and amplitude increases) that we observe on both optical sensors are truly refraction index changes measurements. Then, the fringes do not seem to be linked to another phenomenon such as vibrations. We can see on Figure 7.b) regions with different contrasts on the spherical shock wave, the half sphere has a greater contrast in the center, which shows a greater variation in refractive index at this precise location. That would confirm the fact that there is more energy in the shock in front of the exit tube compared the sides of the half sphere. The sides of the spherical shock that arrive on the SMI sensor and the reflector are clearer on the shadowgraph. The Figure 7.c) and Figure 7.d) display the next steps of the spherical wave propagation. Between t_1 and t_2, the average pressure along the laser beam would be fairly constant while a one-point measurement like P_r would clearly see a peak then a decay.

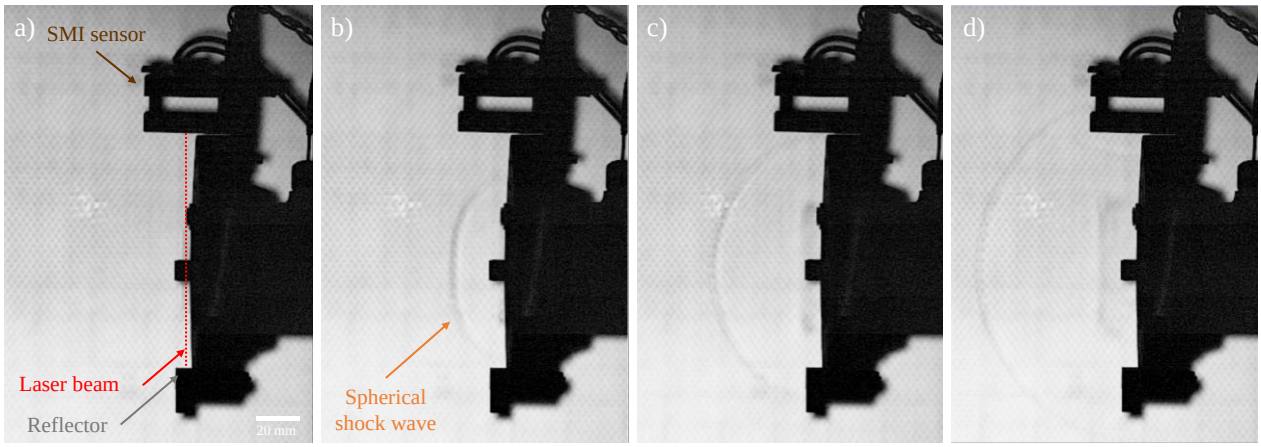

Figure 7 : Shadowgraphy images at the exit of the open shock tube for shock wave shape observation at $t_1 = t_0 + 860$ µs (a), $t_2 = t_0 + 900$ µs (b), $t_3 = t_0 + 950$ µs (c) and $t_4 = t_0 + 1$ ms (d).

4. CONCLUSION

In this paper, we compared two types of refractive index measurement systems in order to obtain the overpressure induced by a shock wave in the air. The SMI and the all-fiber Michelson interferometer were presented, each with its own processing method: fringe counting and triature phase analysis respectively. Both measurement methods were used for incident pressure measurements in the driven chamber and at the exit of laboratory shock tube open at the end of the driven section. Those measurement locations give different refractive index spatial distribution; an optical incident pressure measurement probes theoretically a planar shock wave, while an optical system at the exit tube measures a refractive index change through a spherical shock wave. The SMI sensor shows coherent overpressure values and good chronometry, in agreement with piezoelectric reference sensors. The interferences fringes for the SMI were more visible for the incident pressure measurement compared to the spherical exit tube shock wave. The raw SMI signals and shadowgraphy imaging suggest that there is a refractive index inhomogeneity of the spherical shock wave. The curvature of the shock wave front influences strongly the fringes of the raw SMI signals and thus the refractive index change seen by each optical sensor. A larger bandwidth for SMI sensors would, result in better fringes to enhance fringe detection. The actual limitation at low pressure level is the pressure resolution, we are currently investigating more advanced signal processing techniques to improve this resolution. The Michelson interferometer results present a correct chronometry but the refractive index amplitudes are largely underestimated on both location along the tube. The refractive index inside the shock tube looks like a continuous step pressure profile, but as the amplitude is not correct, this is questionable. Currently, this behavior is not understood. In order to understand this, other optical probes and interferometer configurations will be evaluated in the near future. Furthermore, these optical sensors will be tested in open field detonation experiments.

REFERENCES

[1] P.L. Walter, “Air-blast and the Science of Dynamic Pressure Measurements”, Sound and Vibration, pp. 10-16, (2004).

[2] J. Riondet, A. Coustou, H. Aubert, P. Pons, M. Lavayssière, J. Luc, A. Lefrançois, “Design of air blast pressure sensors based on miniature silicon membrane and piezoresistive gauges”, J. Phys.: Conf. Ser. 922 012019 (2017)

[3] G. Guerke, “Evaluation of Blast Pressure Measurements”, Bericht des Ernst-Mach-Instituts, 90, 3, Seo. (1990)

[4] K. Bertling, J. Perchoux, T. Taimre, R. Malkin, D. Robert, A.D. Raki’c, T. Bosch, “Imaging of acoustic fields using optical feedback interferometry”, Optics express (2014), 22, 30346–30356

[5] J. Devlaminck, J.Luc, and P.-Y.Chanal, “Digital signal processing for velocity measurements in dynamical material's behaviour studies”, Sci. Instrum. 85, 035109 (2014)

[6] R. Lang, K. Kobayashi, “External Optical Feedback Effects on Semiconductor Injection Laser”, 71 Properties. J. of Quan. Electron. (1980), QE-16, 347–355

[7] K. Petermann, “Laser diode modulation and noise”, Vol. 3, Springer Science & Business Media, (1991)

[8] J.A. Roumy, J. Perchoux, Y.L. Lim, T. Taimre, A.D. Raki´c, T. Bosch, “Effect of injection current and temperature on signal strength in a laser diode optical feedback interferometer”, Appl. Opt. (2015), 54, 312–318

[9] S. Maqueda, J. Perchoux, C. Tronche, J. J. Imas González, M. Genetier, M. Lavayssière, and Y. Barbarin, “Demonstration of pressure wave observation by acousto-optic sensing using a self-mixing interferometer”, Sensors 23 (7), 3720 (2023)

[10] O.T. Strand, D.R. Goosman, C. Martinez, and T. L. Whitworth, “Compact system for high-speed velocimetry using heterodyne techniques”, Review of Scientific Instruments 77, 083108, (2006)

[11] P. Mercier, J. Benier, A. Azzolina, J. Lagrange, and D. Partouche, “Photonic Doppler velocimetry in shock physics experiments”, J. Phys. IV134,805–812, (2006)

[12] J. Weng, H. Tan, X. Wang, Y. Ma, S. Hu, X. Wang, “Optical-fiber interferometer for velocity measurements with picosecond resolution”, Applied Physics Letters 89, 111101, (2006)

[13] D.H. Dolan, S.C. Jones, “Push-pull analysis of photonic Doppler velocimetry measurements”, Review of Scientific Instruments 78, 076102, (2007)

[14] G. Le Blanc, S. Bergey, J. Vich, T. d'Almeida, M. Roudot, J. Luc, Y. Barbarin, "532-nm triature Photonic Doppler Velocimetry", Proc. SPIE 12016, Optical and Quantum Sensing and Precision Metrology II, 120160X (2022)

[15] S. Downes, A. Knott, I. Robinson “Towards a shock tube method for the dynamic calibration of pressure sensors”, PTRSL A: Mathematical, Physical and Engineering Sciences 372 (2014)

[16] C. Sarraf, J.-P. Damion “Dynamic pressure sensitivity determination with Mach number method”, Measurement Science and Technology 29(5): 054006. (2018).